ISSN 1047-8477
Volume 161, Number 1, January 2008

Journal of Structural Biology

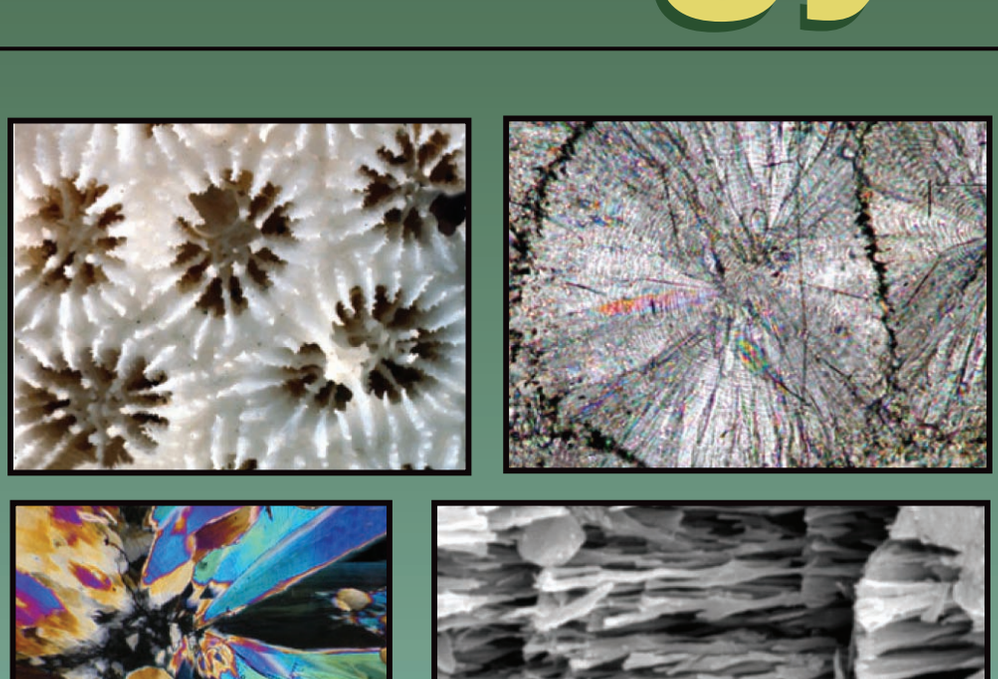

Available online at www.sciencedirect.com
ScienceDirect
Journal of Structural Biology 161 (2008) 74–82
Journal of Structural Biology
www.elsevier.com/locate/yjsbi

Hierarchically structured scleractinian coral biocrystals

Radosław Przeniosło [a,*], Jarosław Stolarski [b], Maciej Mazur [c], Michela Brunelli [d]

[a] Institute of Experimental Physics, University of Warsaw, Hoża 69, PL-00-681 Warsaw, Poland
[b] Institute of Paleobiology, Polish Academy of Sciences, Twarda 51/55, PL-00-818 Warsaw, Poland
[c] Department of Chemistry, Laboratory of Electrochemistry, University of Warsaw, Pasteura 1, PL-02-093 Warsaw, Poland
[d] European Synchrotron Radiation Facility, BP 220, F-38043 Grenoble, France

Received 25 May 2007; received in revised form 18 September 2007; accepted 19 September 2007
Available online 5 October 2007

Abstract

Microscopic (AFM and FESEM) observations show that scleractinian coral biomineral fibers in extant *Desmophyllum* and *Favia*, and fossil Jurassic *Isastrea* are composed of nanocrystalline grains of about 30–100 nm in size. In contrast to these findings, SR diffraction data on the same coral materials exhibit narrow Bragg peaks suggesting much larger crystallite size. These seemingly contradicting results of microscopic and diffraction studies are reconciled within a new, minute-scale model of scleractinian biomineral fibers. In this model, nanocrystalline aragonite units are interconnected by mineral bridges and form aggregates usually larger than 200 nm. Most likely, the size of the aggregates is resulting from physiological biomineralization cycles that control cellular secretion of ions and biopolymeric species. Intercalation of biopolymers into crystal lattice may influence consistently several structural parameters of the scleractinian coral bio-aragonite in all studied samples: (i) the lattice parameters and internal strains of the bio-aragonite are larger than in mineral aragonite, (ii) lattice parameter elongations and internal strains reveal directional anisotropy with respect to crystallographic axes.

Keywords: Biominerals; Scleractinian corals; *Desmophyllum*; *Favia*; *Isastrea*; $CaCO_3$; Aragonite; Synchrotron radiation diffraction; X-ray diffraction; SEM; AFM

1. Introduction

Reef-building scleractinian corals belong to the most extensive natural producers of $CaCO_3$ (Milliman, 1993). Modern scleractinian corals produce carbonate skeleton whose principal polymorph is aragonite (see also Stolarski et al., 2007a). Until recently it has been commonly assumed that biological control of skeleton formation is confined to the initiation of its growth (in the regions called calcification centers) whereas the successive growth of biomineral fibers follows strictly physico-chemical rules of abiotic crystal growth resembling the formation of $CaCO_3$ marine cements (Bryan and Hill, 1942; Constantz, 1986). It was a "single orthorhombic crystal of aragonite" that was considered fundamental unit of coral skeleton (Bryan and Hill, 1942: 84). This purely inorganic model of fibers growth is particularly persuasive when the optical behavior (extinction every 90° as the specimen is rotated) of fibers in the polarized light is observed (Wainwright, 1964).

However, the early claims as to the monocrystalline aragonite ($CaCO_3$) structure of fibers have been challenged by the results of X-ray micro-diffraction that documented their polycrystalline nature. Wainwright (1964) observed the orientation of the aragonite crystallites along the crystallographic *c* axis, the *a* and *b* directions being randomly distributed. The interpretation of fibers as purely inorganic polycrystals has been also challenged by nanostructural atomic force microscopy (AFM) observations which point to their nanocomposite structure. Mineral nanograins, ca. 30–100 nm in diameter (Stolarski, 2003; Cuif et al., 2004; Cuif and Dauphin, 2005a,b; Stolarski and Mazur, 2005;

* Corresponding author. Fax: +48 22 628 7252.
E-mail addresses: radek@fuw.edu.pl (R. Przeniosło), stolacy@twarda.pan.pl (J. Stolarski), mmazur@chem.uw.edu.pl (M. Mazur), brunelli@esrf.fr (M. Brunelli).

1047-8477/$ - see front matter © 2007 Elsevier Inc. All rights reserved.
doi:10.1016/j.jsb.2007.09.020

Dauphin et al., 2006), are embedded in a "thin layer of a highly interactive (i.e., organic) material" (Cuif and Dauphin, 2005b). Even deeper penetration of the mineral structure by the organic components is suggested by high-resolution synchrotron radiation (SR) diffraction studies. Bio-aragonite extracted from corals (Stolarski et al., 2007b) reveal anisotropic elongation of the lattice parameters *a*/*b*/*c* similar to that previously reported for biogenic aragonite extracted from bivalve, gastropod and cephalopod shells (Pokroy et al., 2004, 2006). Also chemical and isotopic composition of scleractinian skeletons is under strong biological control (Rollion-Bard et al., 2003; Allison et al., 2005; Meibom et al., 2006, 2007). These new evidences support the view that in contrast to synthetic, abiotically precipitated $CaCO_3$, structure of scleractinian coral bio-aragonite is, from the macroscopic down to the atomic length scales, influenced by organic macromolecules present in biomineralization region. Similar biological control on hierarchical structure of biominerals has been described in variety of organisms (Aizenberg et al., 2005; Fantner et al., 2005; Tai et al., 2006; Oaki et al., 2006).

One of the basic questions raised by nanostructural observations concerns the mechanisms that arrange nanocrystals into crystallographically continuous units ("skeletal fibers"). Up to now, the nanoscale morphology of scleractinian coral biocrystals has been investigated only over relatively small areas (ca. 2 μm^2), and the larger scale, hierarchical arrangement of the nanograins (i.e., their organization in higher level structural units) has not been accurately described and/or still needs to be verified by preparation-free methods (Dauphin et al., 2006). In this paper, we present for the first time the quantitative analysis of the mineral nanocomponents based on high-resolution synchrotron radiation diffraction studies. We also propose a model of the minute-scale hierarchical structure of the scleractinian coral skeleton that is based on combined SR diffraction data and nanotopographic field emission scanning electron microscopy (FESEM) and AFM observations performed over micrometer range scales.

2. Material and methods

2.1. Samples

Biomineral samples were extracted from the skeletons of three scleractinian coral species: (1) *Favia stelligera* (Dana, 1846), extant colonial, shallow-water, and zooxanthellate coral (collection site: Lizard Island, Great Barrier Reef, Pacific Ocean, 5–10 m; ZPAL V.31/1), (2) *Desmophyllum dianthus* (Esper, 1794), extant solitary, deep-water, azooxanthellate coral (collection site: off Chile, station: 51052, Pacific Ocean, 51°52,0′S/73°41,0′W; 636 m; ZPAL H.25/5-Car), and unusually well preserved (3) *Isastrea* cf. *bernensis* Etallon, 1864, fossil, colonial, presumably shallow-water coral from the Oxfordian (Upper Jurassic) deposits of western Pomerania that still preserves aragonite skeleton mineralogy (collection site: Ostromice, Poland, see Roniewicz, 1984; ZPAL H.IV/303). In the text, for brevity, only generic names of species are mentioned (i.e., *Favia*, *Desmophyllum* and *Isastrea*). The reference Geological Aragonite (ZPAL V.31/10/VMIN08) came from Tazouta Mine in the Atlas Mountians, Morocco (Sefrou, Sefrou Prefecture, Fès-Boulemane Region). All samples are housed in the Institute of Paleobiology, Polish Academy of Sciences, Warsaw (abbreviation ZPAL).

2.2. Microscopic techniques

Atomic Force Microscopy was performed on MultiMode Nanoscope IIIa (Digital Instruments, Veeco). Standard silicone nitride cantilevers were used for measurements in contact mode. The coral samples extracted *en bloc* from the skeleton were polished with diamond suspension of grain sizes 5 and 1 μm, and then with aluminium oxide (Buehler Topol 3 final polishing suspension with particle size 0.25 μm). After polishing, the sections were rinsed in Milli-Q water and washed in an ultrasonic cleaner for 10 s. The polished samples were then etched in 1% ammonium persulfate in McIlvain buffer (pH 8) for 10 min. Next, they were rinsed with deionized water and dried.

Scanning Electron Microscopy was performed on Philips XL 20 SEM or Field Emission SEM LEO1530. For standard SEM measurements polished and etched blocks of corals skeleton were used. The preparation procedure involved polishing the samples with diamond powder 1200 Grit and aluminium oxide (Buehler Topol) followed by etching for 10 s in 0.1% formic acid. High resolution FESEM imaging was performed on fractured native septa extracted from coral skeletons.

Laser Confocal Scanning Fluorescence Microscope observations of *Desmophyllum* section (Fig. 6) were acquired on a Leica TCS SP1 Confocal Microscope at the Natural History Museum, London. Polished section was stained in a 0.45 μm filtered 1% acridine orange aqueous solution for 5 min, then briefly rinsed in distilled water and air dried. Argon laser operating at 488 nm was used to excite fluorescence which was detected at 500–600 nm.

2.3. Synchrotron radiation high resolution powder diffraction

Measurements were performed at the beamline ID31 at (Fitch, 2004) ESRF Grenoble. Samples of the extant *Desmophyllum* and *Favia*, were extracted *en bloc* from the skeleton as approximately parallelepiped pieces ($4 \times 4 \times 1$ mm) and mounted directly in transmission mode in the SR beam. The samples consisted of septa/wall parts whose microstructural units (fibers) have different orientation. The coral sample was immobile during the measurements. SR measurements were also performed for pulverized biogenic fossil *Isastrea* and pulverized reference Geological Aragonite. Both pulverized samples were sealed in borosilicate capillaries 0.7 mm and 1.0 mm in diameters, respectively. The capillaries were rotated during the

measurements to minimize the texture effects. The wavelength value was refined from measurements with a Si sample (NIST standard). The diffractometer resolution was estimated from measurements with LaB_6. The following wavelengths were used: 0.30020(4) Å for *Desmophyllum*, *Isastrea* and Geological Aragonite, 0.30001(2) Å for *Favia*. The Rietveld refinements were done with FullProf software (Rodriguez-Carvajal, 1993) in order to determine the lattice parameters. Information about the microstructure was obtained by fitting individual Bragg peaks with a pseudo-Voigt function and strain-size analysis based on the Williamson–Hall method (Williamson and Hall, 1953).

Sr content in examined samples was calculated using Energy Dispersive Spectroscopy (EDS) performed on a Philips XL-20 scanning microscope coupled with the EDS detector ECON 6, system EDX-DX4i.

3. Results

The macro- and microscopic skeletal features of the extant *D. dianthus*, *F. stelligera* and fossil (Jurassic) *Isastrea* cf. *bernensis* are shown in Fig. 1A, B and C, respectively. In transverse sections through the septa (Fig. 1A_{2-4}–C_{2-4}) two main regions are clearly visible: calcification centers and radiating fiber bundles. Fibers are formed by the sequential addition of micrometer-sized growth layers. Ordered crystallographic structure of the fibers is indicated by complete light extinction every 90° during rotation of the specimen in polarization microscope (Fig. 1A_3–C_3).

The low FESEM magnifications of naturally fractured corallum (thickening deposits of the septum) (Stolarski, 2003) show linearly arranged skeletal fibers which are almost parallel to each other (Fig. 2A_1–C_1). The fibers show a bumpy surface exhibiting a discrete nanogranular morphology (Fig. 2A_2–C_2). However, the nanograins are not distinctly separated from each other and usually form clusters a few hundred nanometers in size. Also the polished and selectively etched samples (organic components removed) reveal nanogranular texture with grains ca. 30–100 nm in diameter. The individual nanograins have a semicircular outline and are usually separated from each other by spaces of a few nanometers. Occasionally, one may also observe larger nanograin clusters ca. 100–200 nm in diameter (e.g., Fig. 2B_3). This microscopic view, obtained from FESEM and AFM measurements, was further compared with high resolution synchrotron radiation diffraction results.

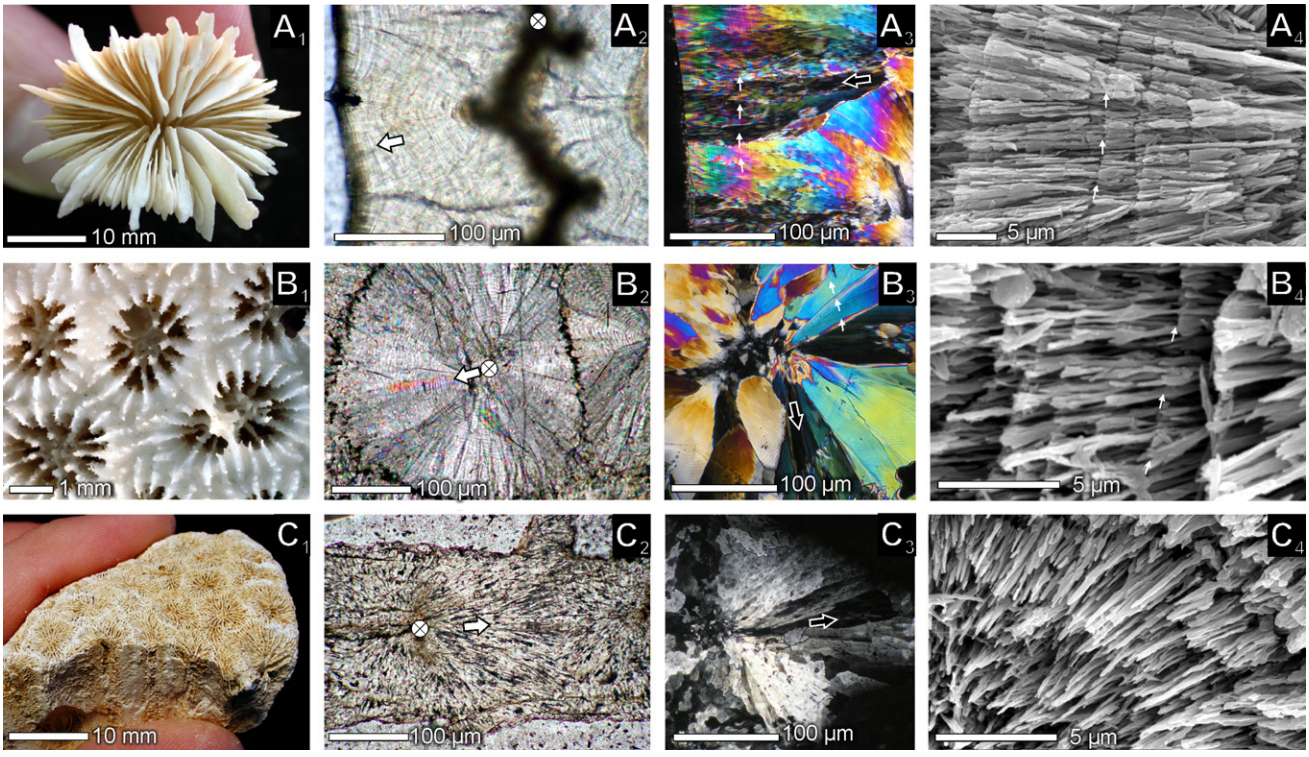

Fig. 1. From macro- to microstructural organization of the scleractinian coral skeleton. Corallum macrophotographs (with subscript "1") followed by images of transverse thin-sections (with subscript"2"), ultra-thin sections in polarized light (with subscript "3"), and Scanning Electron Microscope (SEM) images of polished and etched sections (with subscript "4") for each of the examined here species: extant *Desmophyllum dianthus* (A), *Favia stelligera* (B) and fossil (Jurassic) *Isastrea* cf. *bernensis* (C). In transverse sections (A_2–C_2), the calcification centers are marked with crossed circles; arrows indicate direction of fiber growth and the approximate position of ultra-thin sectioned skeletal regions. Complete light extinction (A_3–C_3, black arrows) of the entire fiber bundle in polarized light indicates similar arrangement of axes of individual crystallographic domains. Incremental growth of fibers (ca. 2–5 μm step) results in division of "individual" fibers into several micrometric sub-units consisting of narrow zones enriched (white arrows in A_3, A_4, and B_3, B_4) and wider zones depleted in organic components; the zones enriched in organics show a stronger negative etching relief (A_4, and B_4); similar zonation of biocrystal fibers can also be observed in skeleton of Jurassic *Isastrea* (white arrows in C_4).

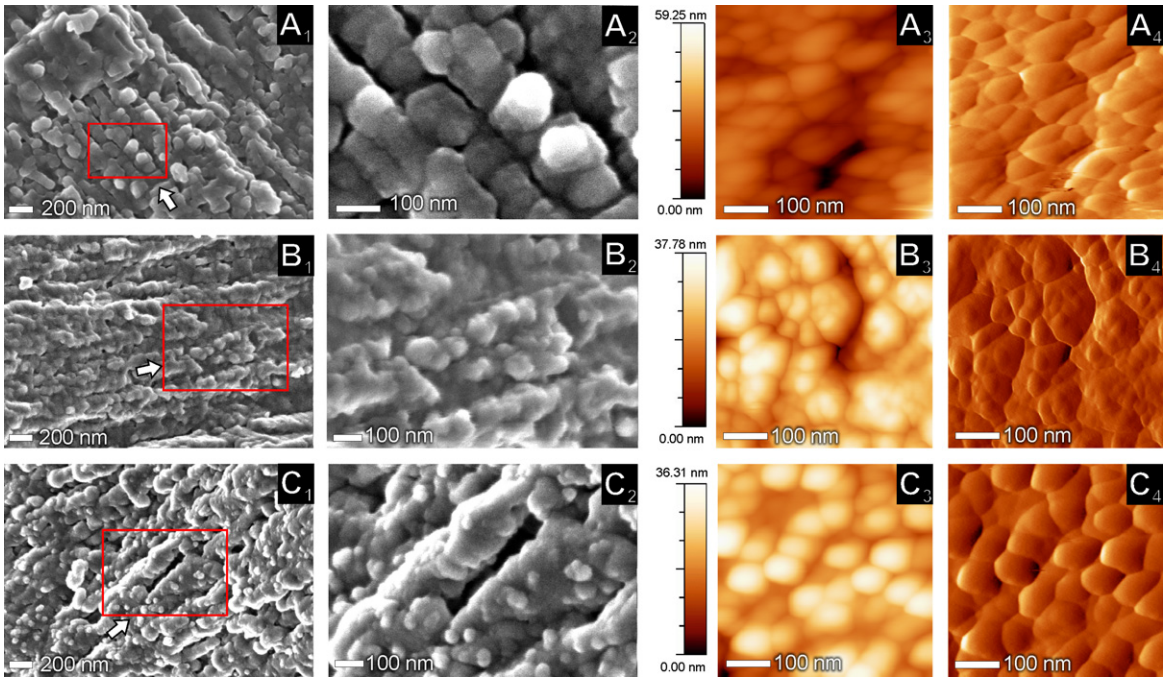

Fig. 2. From micro- to nanostructural organization of the scleractinian coral skeleton. Field Emission Scanning Electron Microscope (FESEM) images of fractured septum (with subscript "1" and "2"; different magnifications) are followed by Atomic Force Microscope (AFM) images (with subscript "3" [height mode, preceded with *z*-scale bar] and "4" [deflection mode]) of fibrous skeleton of each of the examined here species: extant *Desmophyllum dianthus* (A) and *Favia stelligera* (B) and fossil (Jurassic) *Isastrea* cf. *bernensis* (C). FESEM images show linear arrangement of nanograins concordant with the longer axis of the skeletal fibers (white arrows in A_1–C_1), i.e., the crystallographic *c*-axis of aragonite.

Based on diffraction data we performed Rietveld analysis of the biogenic and reference mineral aragonite samples. The analysis was done by assuming the aragonite structure, and the atomic positions taken from Caspi et al. (2005) were fixed while the lattice parameters were refined. In the case of *Favia* we assumed a minute amount of calcite structure (Maslen et al., 1995), while the other samples i.e., *Desmophyllum*, *Isastrea* and the reference mineral, were treated as pure aragonite since they did not show Bragg peaks due to other polymorphic phases. As it was suggested by previous studies (Greegor et al., 1997), scleractinian coralla may also contain strontianite $SrCO_3$ in amounts of ca. 3000 ppm. We simulated the SR diffraction pattern assuming the crystal structure of $SrCO_3$ (Villiers de, 1971) and compared the intensities of the most intense Bragg peaks with the background fluctuation observed in the corals' diffraction patterns. We do not see any peaks that might be due to $SrCO_3$ so we can assume that the $SrCO_3$ content does not exceed: 0.1% (*Favia*), 0.1% (*Desmophyllum*), and 0.2% (*Isastrea*). The resulting lattice parameters of aragonite determined for our biogenic samples are compared with the reference aragonite data (Caspi et al., 2005) as shown in Table 1. The influence of the small Sr content on the lattice parameters of the aragonite samples under study, with formula $Ca_{1-x}Sr_xCO_3$ ($x < 0.0035$), is shown in Fig. 3. The lattice parameters for biogenic samples (solid symbols) and geological aragonite samples (open symbols) are shown as a function of Sr content x. Both solid and dotted lines have the same slope taken from studies of the $Ca_{1-x}Sr_xCO_3$ compounds (Lucas-Girot et al., 2007). Absolute values of the lattice parameters for $Ca_{1-x}Sr_xCO_3$ with $x = 0.001$ given in (Lucas-Girot et al., 2007) fall outside our plots. Therefore in Fig. 3 we show two lines with the same slope but different intercepts. The solid and dotted lines pass through the datapoint from geological reference aragonite (Caspi et al., 2005) and from herein examined geological aragonite, respectively. We do not know what is the reason of the slight discrepancy between the results for both geological aragonite samples. It is however important to note that all our biogenic samples show lattice parameter elongations which are larger than those expected because of the increased Sr content.

In order to characterize the microstructure of the samples we fitted each Bragg peak to a pseudo-Voigt function. All Bragg peaks can be well described by a pseudo-Voigt function with the parameter η: $0.8 < \eta < 1.0$. We selected three groups of peaks with scattering vector Q direction almost parallel to a^*, b^* and c^* directions, respectively (shown in Fig. 4 in blue, green and red colour). The criterion of selection was that $\cos(\alpha_i) > 0.9$, where α_i is the angle between Q and a^*, b^* or c^* for $i = 1,2,3$, respectively. The (Williamson and Hall, 1953) plots in Fig. 4 show the square of the integral breadth β^2 as a function of the square of the scattering vector Q^2 for all three groups of Bragg peaks. The data for each group were fitted to the linear function:

$$\beta^2(Q) = \beta_0^2 + AQ^2$$

In further analysis we assume that the interplanar distances, d, in the sample have a normal distribution around the average value $\langle d \rangle$ with a distribution σ:

Table 1
Structural parameters for biogenic aragonite from extant *Desmophyllum*, *Favia* and fossil (Jurassic) *Isastrea*, and of the reference geological aragonite

	1 d (Å)	2 $\Delta d/d_{ref}$ (%)	3 ε (%)	4 L (nm)
Desmophyllum a	4.96682(3)	0.101(1)	0.043(1)	>400
Desmophyllum b	7.97443(4)	0.066(1)	0.051(6)	>300
Desmophyllum c	5.75158(3)	0.135(1)	0.057(5)	250(100)
Favia a	4.96509(2)	0.066(1)	0.037(1)	180(10)
Favia b	7.97226(3)	0.039(1)	0.043(6)	130(20)
Favia c	5.75004(2)	0.125(1)	0.051(9)	220(80)
Isastrea a	4.96538(2)	0.072(1)	0.041(4)	220(30)
Isastrea b	7.97480(3)	0.071(1)	0.052(6)	170(30)
Isastrea c	5.74853(2)	0.100(1)	0.056(3)	230(20)
Geological aragonite a	4.96394(1)	0.043(1)	0.037(8)	>400
Geological aragonite b	7.97139(2)	0.028(1)	0.032(13)	200(70)
Geological aragonite c	5.74528(1)	0.042(1)	0.018(8)	250(50)

The lattice parameters (column 1), the relative elongation as compared with the geological aragonite reference (Caspi et al., 2005) (column 2). The internal strain and average grain size are given in columns 3 and 4, respectively.

$$N(d) = \frac{1}{\sigma\sqrt{2\pi}} \exp\left(\frac{(d - \langle d\rangle)^2}{2\sigma^2}\right)$$

From the Williamson–Hall fits we estimate the average strain in the three main directions: $\varepsilon_i = \sigma_i/\langle d_i\rangle$ where d_i stands for a, b and c lattice parameter for $i = 1$, 2 and 3, respectively. The strain values are calculated from the slope parameter A:

$$\varepsilon = \sqrt{\frac{A}{2\pi}}$$

The average grain size L is estimated from the Scherrer formula assuming $K = 0.9$:

$$L = 2\pi K/\beta_0$$

The values of strains ε and grain sizes L are given in Table 1.

Anisotropic elongation of the aragonite lattice parameters is observed in biogenic samples, which is in good agreement with our previous diffraction studies of coral samples (Stolarski et al., 2007b) as well as with literature reports on bivalve, gastropod and cephalopod shells (Pokroy et al., 2004, 2006). All relative elongations are positive and the larger, medium and smaller values correspond to the c, a and b axes, respectively. Noteworthy, the geological aragonite reference sample yields lattice parameters that differ from those previously published (Caspi et al., 2005). However, the relative difference between these two mineral samples is 0.03–0.04%, which is much less than that between biogenic and mineral aragonite.

It is clearly seen in Fig. 4 that the internal strains in biogenic samples are anisotropic and show similar values for each direction in all three biogenic samples. They all differ considerably from the geological aragonite case. In the biogenic shells the average strain along the a axis is considerably smaller than that observed along the b and c axes. By comparing the relative lattice parameter elongation with the average lattice strain in the same direction, i.e. $\Delta a/a$ to ε_a and $\Delta c/c$ to ε_c, one can conclude that only a small part of the sample volume (no more than a few percent) exhibits lattice parameters a and c equal to the values of the reference geological aragonite (Caspi et al., 2005). The important conclusion from this finding is that the strong lattice parameter elongation for the a and c directions occurs within the whole aragonite lattice of the biomineral.

4. Discussion

The average grain size determined from SR diffraction data is in the order of 200–250 nm, i.e., considerably higher than the size of the nanograins observed in FESEM and AFM (30–100 nm). Both SR diffraction and microscopic observations can be coherently interpreted assuming the model of nanocrystals interconnected by crystalline bridges (Oaki et al., 2006; Oaki and Imai, 2005). Following Oaki

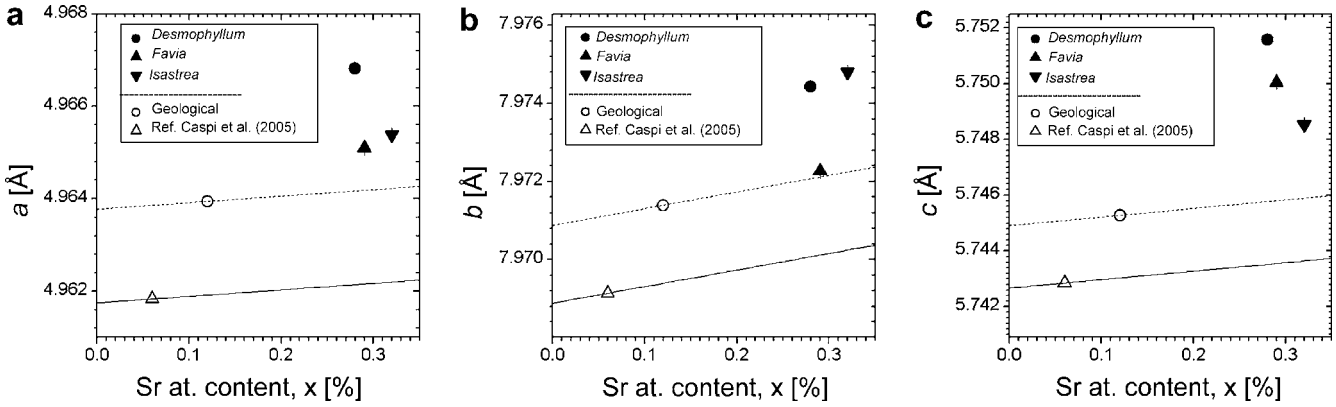

Fig. 3. Values of the aragonite lattice parameters a, b, c (a, b, c, respectively) as a function of Sr content, x in $Ca_{1-x}Sr_xCO_3$. Results for biogenic samples from *Desmophyllum* (●), *Favia* (▲) and *Isastrea* (▼) are compared with those for geological sample from (Caspi et al., 2005) (Δ) and our geological sample (O). The lines show the lattice parameters' dependence on x, with the slope taken from Lucas-Girot et al. (2007). The intercept of the solid and dotted lines is arbitrarily chosen to pass through the data point from (Caspi et al., 2005) and our geological sample, respectively.

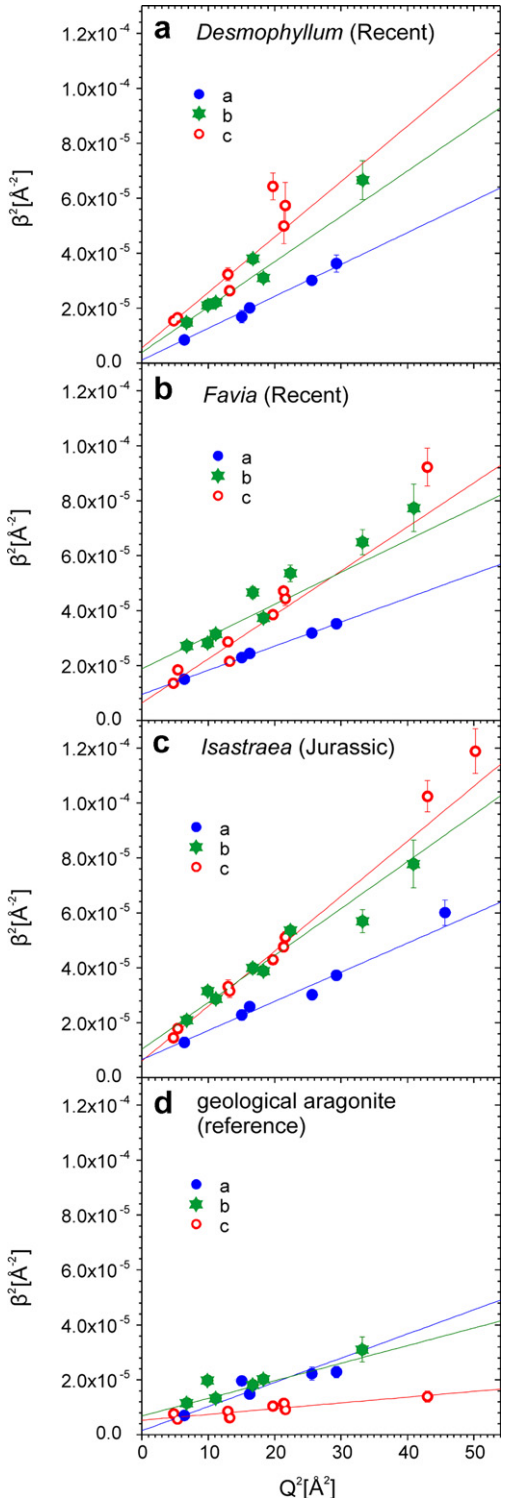

Fig. 4. Williamson–Hall plots showing the square of the integral breadth β^2 as a function of the square of the scattering vector Q^2 (both in $Å^{-2}$). Panels from top to bottom show data for biogenic *Desmophyllum* (a), *Favia* (b), *Isastrea* (c), and reference geological aragonite (d). Solid circles denote experimental data for Bragg peaks with scattering vectors Q directed almost parallel to the a^* (blue) b^* (green) and c^* (red) directions (i.e. when $\cos(Q,a^*) > 0.9$, etc.) The lines show fitted linear functions for the corresponding direction (see Eq. (1)).

et al. (2006) we assume that both the nanocrystalline bricks and the linking bridges are composed of atoms arranged in

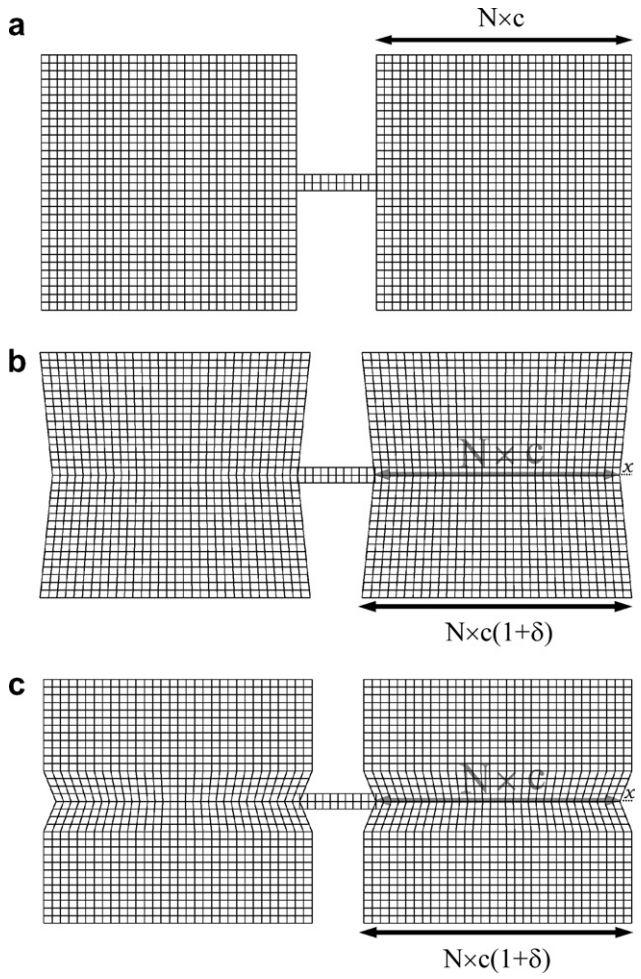

Fig. 5. Schematic representation of two bridged nanocrystals of aragonite. The horizontal and vertical grid lines denote the unit cell edges along c and b crystal axes, respectively. The nanocrystal on the right hand side is composed of N atoms along the c axis direction. For undistorted nanocrystals (a) there are no changes of the lattice spacings through the volume and both bridged nanocrystals can be considered as a single crystal where some small parts around the bridge were as if removed. Distorted nanocrystals (b and c) show an increase of the lattice parameter from c at the central line (along the bridge) up to $c(1 + \delta)$ at the top and bottom edges. In (b) the increase is linear while in (c) it is linear and later constant. Space between nanocrystals is filled with organic components.

the same way as in a single crystal. A diffraction experiment performed on an assembly of such bridged nanocrystals yields narrow peaks since the average grain size is equal to the length of several bricks. A quasi-linear arrangement of possibly bridged nanocrystals can be seen in Fig. 2A_1–C_1. In the case of regular undistorted bricks (Fig. 5a) the diffraction measurement should provide small variations of the lattice parameters and small internal strain values. However, our experimental data for biogenic aragonite are best described when distorted nanocrystals are assumed. Two varieties of the distorted nanocrystal model are shown schematically in Fig. 5b and c.

The distorted nanocrystal model assumes a compression strain of the organic cluster region and tensile strain on those parts of the nanocrystal which are away from the mineral bridge. If the cavity between the nanocrystalline bricks is

filled with organic material, which is less stiff than aragonite it is possible that the equilibrium of forces acting on the nanocrystal edges leads to a distortion similar to that shown in Fig. 5b and c. In both model varieties it is assumed that the lattice parameter along the mineral bridge is equal to c. At the top and bottom edges of the nanocrystal the lattice parameter is equal $c(1 + \delta)$, i.e. slightly larger than c. The two model varieties (Fig. 5b and c) have a different spatial lattice parameter variation: in Fig. 5b the increase is linear while in Fig. 5c there is a linear increase followed by a plateau. Noteworthy, the values of δ cannot be too large, otherwise one would observe broad and asymmetric Bragg peaks which are not observed in our experimental data. The value of δ should be lower than the observed values of $\Delta c/c \approx 0.10\%$. To make the estimation realistic let us consider nanocrystals composed of $N = 100$ atoms along the c direction ($c = 5.75$ Å) of the total length of about 60 nm. In such a case the elongation of the top and bottom edges of the nanocrystal, $x = N\,c\,\delta/2 \approx 0.28$ Å (see Fig. 5b) which is much less than the lattice parameter c.

Both model varieties (Fig. 5b and c) of distorted nanocrystals are idealized and the morphology of the real bioaragonite might be more complex. There may be also an unknown distribution of nanocrystal sizes with an unknown distribution of the δ values in all three directions.

The model of bridged nanocrystals provides plausible explanation of small nanocrystalline grains observed in FESEM and AFM, and an apparently much larger grain size estimated from high resolution SR diffraction measurements. The assumption of distorted nanocrystalline bricks explains the simultaneous occurrence of lattice parameter elongation and the internal strains observed in diffraction measurements. The anisotropic lattice parameter elongation $\Delta d/d$ has the same sequence for all biogenic samples: $(\Delta d/d)_b < (\Delta d/d)_a < (\Delta d/d)_c$. The largest ε and $\Delta d/d$ is observed for the c-direction, which is parallel to the main fiber axis. Noteworthy, the sequence of internal strain values: $\varepsilon_a < \varepsilon_b < \varepsilon_c$ is the same as that of aragonite thermal expansion coefficients around room temperature (Lucas et al., 1999): $\alpha_a < \alpha_b < \alpha_c$ with values of (8.8 ± 1), (19.2 ± 1.7) and $(22.8 \pm 0.3) \times 10^{-6}\ K^{-1}$.

The intriguing aspect of our results is that both extant and fossil $CaCO_3$ biominerals, differing in age by about 150 millions of years, show a similar lattice distortion effect. Such a long-term preservation of the "vital effect" in the biomineral crystalline lattice may appear to be a valuable contribution to astrobiological methodology that allows assessment of the biogenic origin of ancient and very small mineral samples.

The model of bridged nanocrystal architecture proposed by Oaki and Imai (2005) assumes interaction of (1) hydrophilic polymers (soluble acidic proteins) that control $CaCO_3$ polymorphism and are responsible for formation and oriented association of miniaturized building nanoblocks, and (2) hydrophobic polymers (polysaccharides, hydrophobic proteins) that inhibit the unlimited assembly of nanobuilding blocks. Both types of polymers were extracted from the scleractinian coralla (Cuif and Dauphin, 2005a) and XANES-maps (Cuif et al., 2003) show that sulfated polysaccharides are included between the micrometric sub-units of fibers (and not within the sub-units) thus making possible their function as inhibitors of fiber's assembly (Fig. 7). No data about the nanometer-scale distribution of polymers are available that would allow precise structural comparison of organics and bridged-nanograins aggregations proposed herein. Preliminary observations of lightly etched skeleton of *Desmophyllum* (Fig. 6) suggest that ca. 250 nm biomineral modules, delineated by organic-enriched boundaries, may correspond to the grains suggested by SR diffraction data. Fine skeletal growth rhythms are also suggested by distinct Sr/Ca variability (well above the analytical precision of the NanoSIMS instrument) occurring within the micrometric sub-units of fibers (Meibom et al., 2007). Such rhythms may correlate with cellular metabolic turnover rates that can be the time span for bridged nanocrystal formation.

The model of scleractinian skeletal fibers proposed herein explains the apparent contradiction between microscopic observations (Fig. 2) that show nanocrystalline grains of about 30–100 nm size and SR diffraction data that show relatively narrow Bragg peaks due to much larger crystallite sizes (Table 1). Further analytical studies

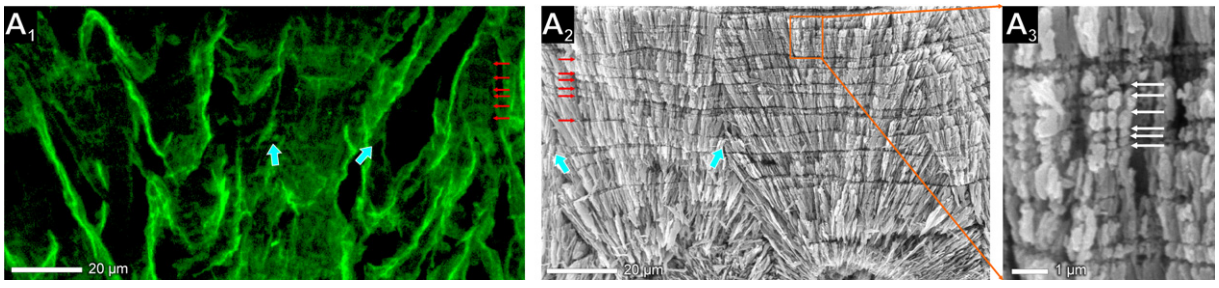

Fig. 6. Fibrous skeleton of *Desmophyllum* in Confocal Laser Scanning Fluorescence Microscope, CLSFM (A_1, organic components stained with acridine orange: vertical organic envelopes of bundles of fibers (blue arrows) and horizontal organic components associated with successive growth increments of fibers (red arrows), and slightly etched in Scanning Electron Microscope, SEM ($A_{2,3}$). Zones enriched in organics typically show a stronger negative etching relief (Stolarski, 2003) and regular growth increments (ca. 2–5 µm step) visualized in CLSFM correspond to distinct interruptions of fibers in SEM (red arrows in $A_{1,2}$). Even smaller incremental steps (ca. 250 nm, white arrows in A_3) are visible in enlarged region of etched skeleton (SEM, A_3) and are below detection limit of CLSFM; these units may correspond to the grain sizes detected by SR diffraction measurements.

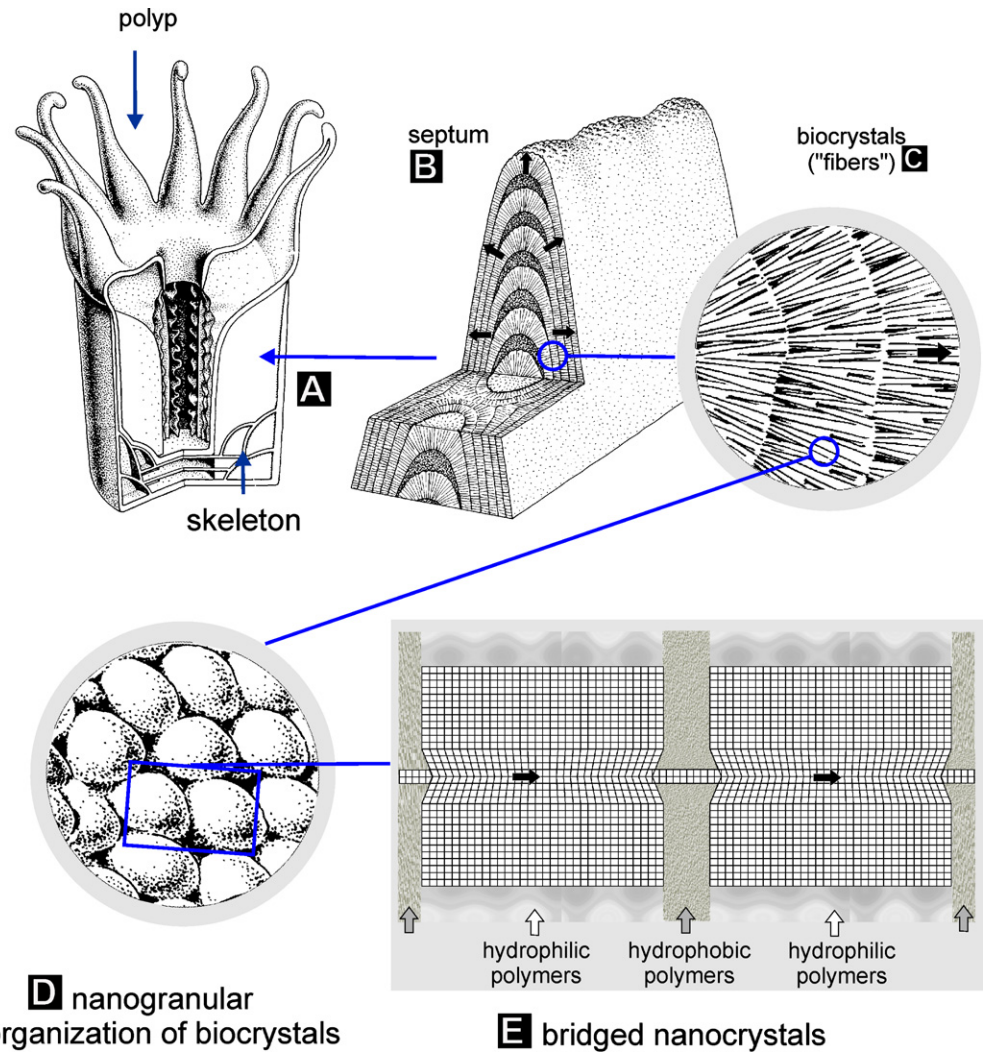

Fig. 7. Idealized model of hierarchical organization of scleractian coral skeleton: from macro- (A), micro- (B and C), nano- (D) to atomic-scale (E). Growth direction of fibrous skeleton is marked with red arrows. Formation of bridged nanograins (E) is interpreted as an interplay between hydrophilic (nanograin formation) and hydrophobic (calcium carbonate inhibitors) polymers secreted rhythmically by the epithelial cells. Crystallographic *c* axis is parallel to the mineral bridges (E).

are planned to visualize the bridge structures and geometrical distortions of the nanocrystalline bricks (idealized in Fig. 5) and to present comprehensive hierarchical model of scleractinian coral skeleton (herein preliminary outlined in Fig. 7).

Acknowledgments

Financial support was provided by the Polish Ministry of Science and Higher Education (R.P.) as well as within projects N307-015733 and 155ESR263. We thank the European Synchrotron Radiation Facility, Grenoble, France for access to experimental facilities. This work was supported by the Synthesis of Systematic Resources EU Program (Project GB-TAF-2213; we thank Drs. Alex Ball and Suzanne Feist-Burkhardt for technical support with CLSM), and the Department of Chemistry, University of Warsaw (Project 120000-501/68-BW-172111). This is the sixth publication of the BIOMIMAT (Biominerals, Biomimetics, Biomaterials) initiative, which aim is to stimulate interdisciplinary research on the origin, evolution, formation, and practical applications of biominerals.

References

Aizenberg, J., Weaver, J.C., Thanawala, M.S., Sundar, V.C., Morse, D.E., Fratzl, P., 2005. Skeleton of Euplectella sp: Structural hierarchy from the nanoscale to the macroscale. Science 309, 275–278.

Allison, N., Finch, A.A., Newville, M., Sutton, S.R., 2005. Strontium in coral aragonite: 3 Sr coordination and geochemistry in relation to skeletal structure. Geochim. Cosmochim. Acta 69, 3801–3811.

Bryan, W.H., Hill, D., 1942. Spherulitic crystallization as a mechanism of skeletal growth in the Hexacorals. Proc. R. Soc. Queensland 52, 78–91.

Caspi, E.N., Pokroy, B., Lee, P.L., Quintana, J.P., Zolotoyabko, E., 2005. On the structure of aragonite. Acta Crystallogr. B. 61, 129–132.

Constantz, B.R., 1986. Coral skeleton construction: a physiochemically dominated process. Palaios 1, 152–157.

Cuif, J.P., Dauphin, Y., 2005a. The environment recording unit in coral skeletons—a synthesis of structural and chemical evidences for a biochemically driven, stepping-growth process in fibers. Biogeosciences 2, 61–73.

Cuif, J.P., Dauphin, Y., 2005b. The two-step mode of growth in the scleractinian coral skeletons from the micrometre to the overall scale. J. Struct. Biol. 150, 319–331.

Cuif, J.P., Dauphin, Y., Berthet, P., Jegoudez, J., 2004. Associated water and organic compounds in coral skeletons: Quantitative thermogravimetry coupled to infrared absorption spectrometry. Geochem. Geophy. Geosy. 5, Q11011. doi:10.1029/2004GC00078.

Cuif, J.P., Dauphin, Y., Doucet, J., Salome, M., Susini, J., 2003. XANES mapping of organic sulfate in three scleractinian coral skeletons. Geochim. Cosmochim. Acta 67, 75–83.

Dauphin, Y., Cuif, J.P., Massard, P., 2006. Persistent organic components in heated coral aragonitic skeletons—Implications for palaeoenvironmental reconstructions. Chem. Geol. 231, 26–37.

Fantner, G.E., Rabinovych, O., Schitter, G., Thurner, P., Kindt, J.H., Finch, M.M., Weaver, J.C., Golde, L.S., Morse, D.E., Lipman, E.A., Rangelow, I.W., Hansma, P.K., 2005. Hierarchical interconnections in the nano-composite material bone: Fibrillar cross-links resist fracture on several length scales. Compos Sci Technol. 66, 1205–1211.

Fitch, A.N., 2004. The high resolution powder diffraction beam line at ESRF. Natl. Inst. Stand. Technol. 109, 133–142.

Greegor, R.B., Pingitore Jr., N.E., Lytle, F.W., 1997. Strontianite in coral skeletal aragonite. Science 275, 1452–1454.

Lucas, A., Mouallem-Bohout, M., Carel, C., Gaudé, J., Matecki, M., 1999. Thermal Expansion of Synthetic Aragonite Condensed Review of Elastic Properties. J. Solid State Chem. 146, 73–78.

Lucas-Girot, A., Hernandez, O., Oudadesse, H., 2007. Re-examination of the structural properties of solid solutions $Sr_xCa_{1-x}CO_3$. Mater. Res. Bull. 42, 1061–1068.

Maslen, E.N., Streltsov, V.A., Streltsova, N.R., Ishizawa, N., 1995. Electron density and optical anisotropy in rhombohedral carbonates III: synchrotron X-ray studies of $CaCO_3$, $MgCO_3$ and $MnCO_3$. Acta Crystallogr. B. 51, 929–939.

Meibom, A., Mostefaoui, S., Cuif, J.P., Dauphin, Y., Houlbreque, F., Dunbar, R., Constantz, B., 2007. Biological forcing controls the chemistry of reef-building coral skeleton. Geophys. Res. Lett. 34. doi:10.1029/2006GL02865.

Meibom, A., Yurimoto, H., Cuif, J.-P., Domart-Coulon, I., Houlbreque, F., Constantz, B., Dauphin, Y., Tambutté, E., Tambutté, S., Allemand, D., Wooden, J., Dunbar, R., 2006. Vital effects in coral skeletal composition display strict three-dimensional control. Geophys. Res. Lett. 33, L11608. doi:10.1029/2006GL02596.

Milliman, J.D., 1993. Production and accumulation of calcium carbonate in the ocean: Budget of a nonsteady state. Global Biogeochem. 7, 927–957.

Oaki, Y., Imai, H., 2005. The hierarchical architecture of nacre and its mimetic material. Angew. Chem. Int. Ed. 44, 6571–6575.

Oaki, Y., Kotachi, A., Miura, T., Imai, H., 2006. Bridged nanocrystals in biominerals and their biomimetics: Classical yet modern crystal growth on the nanoscale. Adv. Funct. Mater. 16, 1633–1639.

Pokroy, B., Fitch, A.N., Lee, P.L., Quintana, J.P., Caspi, E.N., Zolotoyabko, E., 2006. Anisotropic lattice distortions in the mollusk-made aragonite: A widespread phenomenon. J. Struct. Biol. 153, 145–150.

Pokroy, B., Quintana, J.P., Caspi, E.N., Berner, A., Zolotoyabko, E., 2004. Anisotropic lattice distortions in biogenic aragonite. Nat. Mater. 3, 900–902.

Rodriguez-Carvajal, J., 1993. Recent advances in magnetic structure determination by neutron powder diffraction. Physica B192, 55–69.

Rollion-Bard, C., Chaussidon, M., France-Lanord, C., 2003. pH control on oxygen isotopic composition of symbiotic corals. Earth. Planet. Sci. Lett. 215, 275–288.

Roniewicz, E., 1984. Aragonitic Jurassic corals from erratic boulders on the South Baltic coasts. Ann. Soc. Geol. Polon. 54, 65–77.

Stolarski, J., 2003. Three-dimensional micro- and nanostructural characteristics of the scleractinian coral skeleton: a biocalcification proxy. Acta Palaeontol. Pol. 48, 497–530.

Stolarski, J., Mazur, M., 2005. Nanostructure of biogenic versus abiogenic calcium carbonate crystals. Acta Palaeontol. Pol. 50, 847–865.

Stolarski, J., Meibom, A., Przeniosło, R., Mazur, M., 2007a. A Cretaceous scleractinian coral with a calcitic skeleton. Science 318, 92–94.

Stolarski, J., Przeniosło, R., Mazur, M., Brunelli, M., 2007b. High-resolution synchrotron radiation studies on natural and thermally annealed scleractinian coral biominerals. J. Appl. Crystal. 40, 2–9.

Tai, K., Ulm, F.-J., Ortiz, C., 2006. Nanogranular origins of the strength of bone. Nano Lett. 6, 2520–2525.

Villiers de, J.P.R., 1971. Crystal structures of aragonite, strontianite, and witherite. Am. Mineral. 56, 758–766.

Wainwright, S.A., 1964. Studies of the mineral phase of coral skeleton. Exp. Cell Res. 34, 213–230.

Williamson, G.K., Hall, W.H., 1953. X-ray line broadening from filed aluminium and Wolfram. Acta Metal. Mater. 1, 22–31.